Optimal Design for Purcell Three-link Swimmer

Laetitia Giraldi, Pierre Martinon, Marta Zoppello

▶ **To cite this version:**

Laetitia Giraldi, Pierre Martinon, Marta Zoppello. Optimal Design for Purcell Three-link Swimmer. 2014. hal-01098501v1

HAL Id: hal-01098501

https://hal.science/hal-01098501v1

Preprint submitted on 25 Dec 2014 (v1), last revised 6 Jan 2016 (v2)

HAL is a multi-disciplinary open access archive for the deposit and dissemination of scientific research documents, whether they are published or not. The documents may come from teaching and research institutions in France or abroad, or from public or private research centers.

L'archive ouverte pluridisciplinaire **HAL**, est destinée au dépôt et à la diffusion de documents scientifiques de niveau recherche, publiés ou non, émanant des établissements d'enseignement et de recherche français ou étrangers, des laboratoires publics ou privés.

Optimal Design for Purcell Three-link Swimmer

Laetitia Giraldi[*], Pierre Martinon[†], Marta Zoppello[‡]

December 28, 2014

Abstract

In this paper we address the question of the optimal design for the Purcell 3-link swimmer. More precisely we investigate the best link length ratio which maximizes its displacement. The dynamics of the swimmer is expressed as an ODE, using the Resistive Force Theory [13]. Among a set of optimal strategies of deformation (strokes), we provide an asymptotic estimate of the displacement for small deformations, from which we derive the optimal link ratio. Numerical simulations are in good agreement with this theoretical estimate, and also cover larger amplitudes of deformation. Compared with the classical design of the Purcell swimmer, we observe a gain in displacement of roughly 60%.

1 Introduction

The study of self-propulsion at microscopic scale is attracting increasing attention in the recent literature both because of its intrinsic biological interest, and for the possible implications on the design of bio-inspired artificial replicas reproducing the functionalities of biological systems (see for instance [15, 9, 14, 11]). At this scale, inertia forces are negligible compared to the viscous ones i.e. low Reynolds number, calling for different swimming strategies than at greater scales. Thus, we assume that the surrounding fluid is governed by Stokes equations which implies that hydrodynamic forces and torques are linear with respect to the swimmer's velocity. In the case of planar flagellar propulsion , the Resistive Force Theory (RFT) provides a simple and concise way to compute a local approximation of hydrodynamic forces and Newton laws (see [13]). The resulting equations can be written as a system of linear ODEs (see [2, 5, 12]). In this paper we focus on one of the first example of micro-swimmer model found in literature: the "three-link swimmer" [18]. This model is still attracting interest in recent studies, see [4, 3]. The structure of the equations of motion leads to establish a connexion between geometrical control theory and micro-swimming (see [16]). In this paper, we address the optimal design issue, namely finding the optimal length ratio between the three links which maximizes displacement of the swimmer. A similar issue has been studied in [19] where a Fourier expansion is used to derive an optimal design. Here, techniques from the control theory are used to approximate the leading order term of the swimmer's displacement. Maximizing this leading term gives a theoretical value for the optimal link ratio. As far as we know, this procedure is original in that context, and could be applied to others models such as the three-sphere swimmer (see [17]).

The paper is organized as follows. Section 2 recalls the equations of motion for the Purcell swimmer. Section 3 presents strokes which maximize the x-displacement, based on previous simulations from [12]. Section 4 details the expansion of the displacement for such strokes at small amplitude. By maximizing the leader term of this expansion, we derive an optimal length ratio. Section 5 shows the numerical simulations whose results are consistent with this theoretical ratio, for both small and large amplitude of deformation.

[*]UMA, ENSTA, France laetitia.giraldi@ensta-paristech.fr.edu

[†]CMAP, Ecole Polytechnique, France

[‡]University di padova, Italia

2 Modeling

Purcell's 3-link swimmer. The 3-link swimmer is modeled by the position of the center of the second stick $\mathbf{x} = (x, y)$, the angle θ between the x-axis and the second stick (the orientation of the swimmer). The shape of the swimmer defined by the two relative angles β_1 and β_3 (see Fig 1). We also denote by L and L_2 the length of the two external arms and central link.

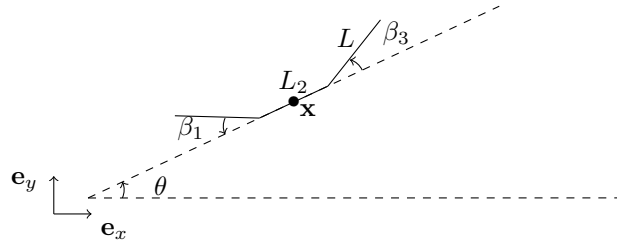

Figure 1: Purcell's 3-link swimmer.

Dynamics via Resistive Force Theory. We approximate the non local hydrodynamic forces exerted by the fluid on the swimmer with local drag forces depending linearly on the velocity. We denote by $\mathbf{e}_i^{\parallel}$ and $\mathbf{e}_i^{\perp}$ the unit vectors parallel and perpendicular to the i-th link, and we also introduce $\mathbf{v}_i(s)$ the velocity of the point at distance s from the extremity of the i-th link, that is

$$\begin{aligned}
\mathbf{v}_1(s) &= \dot{\mathbf{x}} - \frac{L_2}{2}\dot{\theta}\mathbf{e}_2^{\perp} - s(\dot{\theta} - \dot{\beta}_1)\mathbf{e}_1^{\perp}, \quad s \in [0, L], \\
\mathbf{v}_2(s) &= \dot{\mathbf{x}} - (s - \frac{L_2}{2})\dot{\theta}\mathbf{e}_2^{\perp}, \quad s \in [0, L_2], \\
\mathbf{v}_3(s) &= \dot{\mathbf{x}} + \frac{L_2}{2}\dot{\theta}\mathbf{e}_2^{\perp} + s(\dot{\theta} - \dot{\beta}_3)\mathbf{e}_3^{\perp}, \quad s \in [0, L].
\end{aligned}$$

The force $\mathbf{f}_i$ acting on the i-th segment is taken as

$$\mathbf{f}_i(s) := -\xi \left(\mathbf{v}_i(s) \cdot \mathbf{e}_i^{\parallel}\right) \mathbf{e}_i^{\parallel} - \eta \left(\mathbf{v}_i(s) \cdot \mathbf{e}_i^{\perp}\right) \mathbf{e}_i^{\perp}, \tag{1}$$

where ξ and η are respectively the drag coefficients in the directions of $\mathbf{e}_i^{\parallel}$ and $\mathbf{e}_i^{\perp}$.
Neglecting inertia forces, Newton laws are written as

$$\begin{cases} \mathbf{F} = 0\,, \\ \mathbf{e}_z \cdot \mathbf{T}_{\mathbf{x}} = 0\,, \end{cases} \tag{2}$$

where $\mathbf{F}$ is the total force exerted on the swimmer by the fluid,

$$\mathbf{F} = \sum_{i=1}^{N} \int_0^{L_i} \mathbf{f}_i(s)\, ds\,, \tag{3}$$

and $\mathbf{T}_{\mathbf{x}}$ is the corresponding total torque computed with respect to the central point $\mathbf{x}$,

$$\mathbf{T}_{\mathbf{x}_1} = \sum_{i=1}^{N} \int_0^{L_i} (\mathbf{x}_i(s) - \mathbf{x}_1) \times \mathbf{f}_i(s)\, ds\,. \tag{4}$$

Since the $\mathbf{f}_i(s)$ are linear in $\dot{\mathbf{x}}$, $\dot{\theta}$, $\dot{\beta}_1$, $\dot{\beta}_3$, the system (2) can be rewritten as

$$\mathbf{A}(\mathbf{z}) \cdot \begin{pmatrix} \dot{\mathbf{x}} \\ \dot{\theta} \end{pmatrix} - \mathbf{B}(\mathbf{z}) \cdot \begin{pmatrix} \dot{\beta}_1 \\ \dot{\beta}_3 \end{pmatrix} = 0, \tag{5}$$

where $\mathbf{z}(t) := (\beta_1, \beta_3, x, y, \theta)(t)^T$. The matrix $\mathbf{A}$ is known as the "Grand Resistance Matrix" and is invertible (see [2]). Then the dynamics of the swimmer is finally expressed as an ODE system

$$\dot{\mathbf{z}}(t) = f(\mathbf{z}, \dot{\beta}_1, \dot{\beta}_3) = \mathbf{g}_1(\mathbf{z}(t))\,\dot{\beta}_1(t) + \mathbf{g}_2(\mathbf{z}(t))\,\dot{\beta}_3(t)\,, \tag{6}$$

where $\begin{pmatrix}\mathbf{g}_1(\mathbf{z}) & \mathbf{g}_2(\mathbf{z})\end{pmatrix} := \begin{pmatrix}\mathbb{I}_2 \\ \mathbf{A}^{-1}(\mathbf{z})\mathbf{B}(\mathbf{z})\end{pmatrix}$ with $\mathbb{I}_2$ the 2×2 identity matrix. The literal expression of the $\mathbf{g}_i$ is quite complicated (several pages).

3 Optimal strokes

Optimal control problem. We are interested in finding a periodic sequence of deformations which maximizes the displacement of the swimmer along the x-axis. More precisely, we optimize both the link length ratio L_2/L and the deformation of the swimmer over time. Taking the deformation speed $\dot{\beta}_{1|3}$ as control functions, we obtain the optimal control problem

$$(OCP)\begin{cases} \max\ x_2(T)\ \text{ s.t.} \\ \dot{\mathbf{z}}(t) = f(\mathbf{z}(t), \dot{\beta}_1, \dot{\beta}_3) \quad \forall t \in [0,T]\,, \\ \dot{\beta}_{1|3} \in \mathbf{U} = [-b, b] \quad \forall t \in [0,T]\,, \\ \beta_{1|3}(t) \in [-a, a] \quad \forall t \in [0,T]\,, \\ x_2(0) = y_2(0) = \theta_2(0) = 0, y_2(T) = \theta_2(T) = 0\,, \\ \beta_{1|3}(0) = \beta_{1|3}(T), \\ 2L + L_2 = c. \end{cases}$$

We set the constraints a and b over the amplitude and deformation speed, as well as the total length c of the swimmer. The final time T is fixed, and the constraint $\beta_{1|3}(0) = \beta_{1|3}(T)$ ensures that the swimmer is in the same configuration at the initial and final time. Note that this condition can be satisfied by either a single stroke or a sequence of strokes. From [12], numerically solving (OCP) typically gives a periodic sequence of identical strokes. Their phase portrait is octagonal, as illustrated on Fig.2, and we will detail how this shape is consistent with optimal control theory.

Pontryagin's Maximum Principle (PMP). We recall here the PMP as it gives some insight on the shape of optimal strokes. This theorem in optimal control introduced by Pontryagin et al. in [7] gives necessary conditions for local optimality. Interested readers can find more information on the PMP in [1, 20]. The PMP is characterized by an Hamiltonian function H that formally depends on the state variables $\mathbf{z}$, the control functions $\dot{\beta}_{1|3}$, and so-called *costate* variables noted $\mathbf{p}$. While originally inspired by the Hamiltonian in mechanics, in the context of optimal control H does not actually correspond to the energy of the system. The costate variables play the part of the generalized velocities in Lagrangian mechanics, and they can be interpreted as Lagrange multipliers (in the sense of constrained optimization) related to the dynamics of the system. Let the Hamiltonian be

$$H(\mathbf{z}, \mathbf{p}, \dot{\beta}_1, \dot{\beta}_3) = \langle \mathbf{p}, \mathbf{g}_1(\mathbf{z})\rangle\,\dot{\beta}_1 + \langle \mathbf{p}, \mathbf{g}_2(\mathbf{z})\rangle\,\dot{\beta}_3. \tag{7}$$

Under the assumption that $\mathbf{g}_{1|2}$ are continuous and C^1 with respect to $\mathbf{z}$, the PMP states that: if $(\mathbf{z}^*, \dot{\beta}_1^*, \dot{\beta}_3^*)$ is a solution of (OCP) then there exists $\mathbf{p}^* \neq 0$ absolutely continuous such that $\dot{\mathbf{z}}^* = H_p(\mathbf{z}^*, \mathbf{p}^*, \dot{\beta}_1^*, \dot{\beta}_3^*)$, $\dot{\mathbf{p}}^* = -H_z(\mathbf{z}^*, \mathbf{p}^*, \dot{\beta}_1^*, \dot{\beta}_3^*)$, $\mathbf{p}^*(T)$ is orthogonal to the cotangent cone of the final conditions at $\mathbf{z}^*(T)$ and $(\dot{\beta}_1^*, \dot{\beta}_3^*)$ maximizes the Hamiltonian for almost every time $t \in [0,T]$.

Bang arcs. The Hamiltonian in (7) is linear in the controls $\dot{\beta}_{1|3}$. If we assume $\langle \mathbf{p}, \mathbf{g}_i(\mathbf{z})\rangle \neq 0$ for $i = 1, 2$ over a time interval, then the optimal control $\dot{\beta}_{1|3^*}$ that maximizes H must be on the boundary of $U = \{(-b,-b), (-b,b), (b,-b), (b,b)\}$. In terms of phase portrait, this corresponds

to diagonal lines.

Constrained arcs. Moreover, we have the constraints on the joint angles $\beta_{1|3}(t) \in [-a, a]$. When one of them is active and $|\beta_i| = a$, the corresponding control $\dot{\beta}_i = 0$. In terms of phase portrait, this gives horizontal or vertical lines.

Symmetries. As stated in [19], we expect optimal strokes to be symmetric with respect to the diagonal axes $\beta_1 = \beta_3$ and $\beta_1 = -\beta_3$. This comes from the equations of motion being linear and time independent. From the linearity, optimal strokes should be invariant by reflection with respect to the axis of the swimmer's body. From time independence, the stroke should be invariant when inverting the arms movement and going backwards in time.

4 Optimal swimmer design

In this section, we express the leader term of the swimmer's displacement for a stroke of small perimeter which satisfies all properties stated in the previous section. We represent the stroke by a closed octagonal curve γ in the phase portrait (β_1, β_3), see Fig. 2.

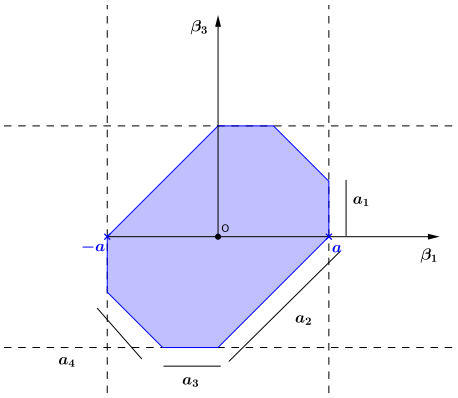

Figure 2: Phase portrait (β_1, β_3) of the octagonal stroke considered for the expansion of the displacement.

As a consequence of neglecting inertia forces, velocities appear linearly in the dynamic, and time can be rescaled without changing the dynamics. Thus the displacement of the swimmer after one stroke does not depend on the speed along the curve γ, but only on the shape of the stroke. From now on, we parametrize γ by the arc-length s. Using a similar approach to [10], we express the swimmer's displacement along the x-axis (i.e., $x(T) - x(0)$) as an asymptotic expansion for small length a_i, $i = 1, \cdots, 4$.

Displacement over the arc $s \in [0, a_1]$. On this part, according to Fig. 2, we set $\mathbf{u} = (\dot{\beta}_1, \dot{\beta}_3) = (0, -1)$. The dynamics of the swimmer is therefore given by $\dot{\mathbf{z}} = -\mathbf{g}_2$, and the time expansion at order two is given by

$$\begin{aligned} \mathbf{z}(a_1) = \quad & \mathbf{z}(0) - a_1 \mathbf{g}_2(\mathbf{z}(0)) \\ & + \frac{a_1^2}{2} \frac{\partial \mathbf{g}_2}{\partial \mathbf{z}} \mathbf{z}(0) \left(\mathbf{g}_2(\mathbf{z}(0))\right) + o(a_1^3)\,. \end{aligned} \tag{8}$$

Displacement over the arc $s \in [a_1, a_1 + a_2]$. Similarly, the position of the swimmer at

$s = a_1 + a_2$ can be expressed as

$$\begin{aligned}\mathbf{z}(a_1 + a_2) = \quad & \mathbf{z}(a_1) - \frac{a_2\sqrt{2}}{2}\mathbf{h}(\mathbf{z}(a_1)) \\ & + \frac{a_2^2}{4}\frac{\partial \mathbf{h}}{\partial \mathbf{z}}\mathbf{z}(a_1)\left(\mathbf{h}(\mathbf{z}(a_1))\right) + o(a_2^3)\,, \end{aligned} \tag{9}$$

where $\mathbf{h} := \mathbf{g}_1 + \mathbf{g}_2$. Plugging the value of $\mathbf{z}(a_1)$ from (8) into (9) and neglecting the terms of order greater than two, we get

$$\begin{aligned}\mathbf{z}(a_1 + a_2) = \quad & \mathbf{z}(0) + c_1(\mathbf{g}_1, \mathbf{g}_2, \mathbf{z}(0), a_1, a_2) \\ & + c_2(\mathbf{g}_1, \mathbf{g}_2, \mathbf{z}(0), a_1, a_2) \\ & + o(a_1^3) + o(a_2^3) \end{aligned} \tag{10}$$

with

$$\begin{aligned} c_1(\mathbf{f}, \mathbf{g}, \mathbf{z}, a_1, a_2) = \quad & -\frac{\sqrt{2}a_2}{2}\mathbf{f}(\mathbf{z}) \\ & + (-a_1 - \frac{\sqrt{2}a_2}{2})\mathbf{g}(\mathbf{z}), \\ c_2(\mathbf{f}, \mathbf{g}, \mathbf{z}, a_1, a_2) = \quad & \frac{a_2^2}{4}\frac{\partial \mathbf{f}}{\partial \mathbf{z}}\mathbf{z}\left(\mathbf{f}(\mathbf{z})\right) + \frac{a_2^2}{4}\frac{\partial \mathbf{g}}{\partial \mathbf{z}}\mathbf{z}\left(\mathbf{f}(\mathbf{z})\right) \\ & + \left(\frac{a_1 a_2\sqrt{2}}{2} + \frac{a_2^2}{4}\right)\frac{\partial \mathbf{f}}{\partial \mathbf{z}}\mathbf{z}\left(\mathbf{g}(\mathbf{z})\right) \\ & + \left(\frac{a_1 a_2\sqrt{2}}{2} + \frac{a_2^2}{4} + \frac{a_1^2}{2}\right)\frac{\partial \mathbf{g}}{\partial \mathbf{z}}\mathbf{z}\left(\mathbf{g}(\mathbf{z})\right). \end{aligned}$$

Displacement over the complete stroke. Iterating the computations along each arc and noting by $P = 2(a_1 + a_2 + a_3 + a_4)$ the stroke perimeter, the expansion of the total displacement for the octagonal stroke is finally obtained as

$$\mathbf{z}(T) - \mathbf{z}(0) = C\ [\mathbf{g}_1, \mathbf{g}_2](\mathbf{z}(0)) + o(a_i^3)_{i=1-4}\,, \tag{11}$$

where

$$C = \frac{a_1 a_2\sqrt{2}}{2} + a_1 a_3 + \frac{a_2 a_3\sqrt{2}}{2} + \frac{a_1 a_4\sqrt{2}}{2} + a_2 a_4 + \frac{a_3 a_4\sqrt{2}}{2}$$

and

$$[\mathbf{g}_1, \mathbf{g}_2](\mathbf{z}(0)) = \nabla\mathbf{g}_2(\mathbf{z}(0)) \cdot \mathbf{g}_1(\mathbf{z}(0)) - \nabla\mathbf{g}_1(\mathbf{z}(0)) \cdot \mathbf{g}_2(\mathbf{z}(0))$$

is the Lie brackets of $\mathbf{g}_1$ and $\mathbf{g}_2$ at point $\mathbf{z}(0)$. Choosing the starting point $\mathbf{z}(0)$ such that $\theta(0) = \beta_1(0) = \beta_3(0) = 0$, we compute the Lie bracket with a formal calculus tool

$$[\mathbf{g}_1, \mathbf{g}_2](0, 0, x, y, 0) = \begin{pmatrix} 0 \\ 0 \\ \frac{\eta - \xi}{\xi}\frac{L^3 L_2(3L + 2L_2)}{(2L + L_2)^4} \\ 0 \\ 0 \end{pmatrix}. \tag{12}$$

Consequently, the x-displacement after one stroke is approximated by

$$x(T) - x(0) = C\left(\frac{\eta - \xi}{\xi}\right)\left(\frac{L^3 L_2(3L + 2L_2)}{(2L + L_2)^4}\right) + o(a_i^3)_{i=1-4} \tag{13}$$

Setting the total length of the swimmer by a constant equal to c, i.e., $2L + L_2 = c$, we find that (13) has a unique maximum at

$$L^* = c\Big(1 - \sqrt{\frac{2}{5}}\Big)\,, \quad L_2^* = c\Big(2\sqrt{\frac{2}{5}} - 1\Big)\,, \tag{14}$$

which gives an optimal ratio of

$$\left(\frac{L_2}{L}\right)^* = \frac{\sqrt{10} - 1}{3} \sim 0.721\,. \tag{15}$$

Remark: in [19] an optimal ratio of 0.747 is given for an efficiency-type criterion. The small gap may be due to the difference in models, or the change of the objective function.

5 Numerical simulations

We solve now the optimal control problem (OCP) numerically, in order to determine the optimal swimming strategy and link ratio. Simulations are performed with the toolbox BOCOP ([8]) that implements a direct transcription method. This approach uses a time discretization to transform the continuous (OCP) into a finite-dimensional optimization problem (nonlinear programming). We refer interested readers to [6] for more details on these methods. We use here an implicit midpoint discretization with 100 to 2500 time steps. Note that this method does not use the PMP.

As stated in (OCP), the criterion is to maximize the total displacement along the x-axis over a fixed time T. The initial state of the swimmer is set as $x(0) = y(0) = \theta_2(0) = 0$, with the final conditions $y(T) = \theta_2(T) = 0$. The initial shape angles are left free, with the periodicity conditions $\beta_i(0) = \beta_i(T), i = 1, 3$. We set the total length $c = 4$ for an easier comparison with the classical Purcell swimmer ($L = 1, L_2 = 2$).

We explore different values for the bounds a, b on the shape angles and deformation speed and see their influence on the optimal stroke and link ratio. For practical applications, the values for a and b should reflect the physical characteristics of the studied swimmer. It should be pointed out that the period of the optimal stroke is not known a priori. We arbitrarily set $T = 1$ in the first set of simulations, and $T = 25$ when studying the larger amplitudes. In the latter case we find that the swimming strategy consists in a periodic sequence of identical strokes, as previously observed in [12].

5.1 Small amplitudes, influence of speed limits

We start with small amplitudes by setting $a = \pi/20$ and solve (OCP) for different values of the speed limit b. Here we set $T = 1$ and use 250 time steps for the discretization. Optimizations take about one minute on a standard laptop. Results are given in Table.1, with the phase portraits for the shape angles β_1, β_3 on Fig.3.

First, we observe that the optimal ratio L_2/L is very close to its theoretical value of 0.721 from (15), regardless of b. The speed bound does however have an influence on the shape of the optimal stroke, and its displacement. Displacement increases with higher speeds, and we find the following empirical relation between b and the stroke shape, confirmed by simulations with other values of a:
- for $b < 4a/T$: diamond stroke, which touches the bound a for the limit case $b = 4a/T$.
- for $4a/T < b < 8a/T$: octagonal stroke.
- for $b = 8a/T$: classical Purcell stroke (square).
- for $b > 8a/T$: sequence of several strokes.

The three strokes observed (diamond, octagon, square) match the discussion from Section 3. They include only diagonal lines (bang arcs saturating the speed limit b) and horizontal/vertical lines (constrained arcs for the amplitude limit a). Note also that the square and diamond strokes are particular cases of the octagonal one, by setting the appropriate arc lengths to 0.

Remark: this empirical relation can also be interpreted in terms of the period T, with the two limit values $T = 8a/b$ for the Purcell stroke and $T = 4a/b$ for the diamond touching a.

Table 1: Small amplitude ($a = \pi/20$).

b	$x(T)$	L_2/L	stroke
0.5	2.68E-3	0.719	diamond
$\pi/5$	4.23E-3	0.719	diamond
0.75	5.70E-3	0.719	octagon
1	7.73E-3	0.719	octagon
$2\pi/5$	8.42E-3	0.717	square
1.5	1.14E-2	0.719	octagon (x2)
2	1.55E-2	0.719	octagon (x2)

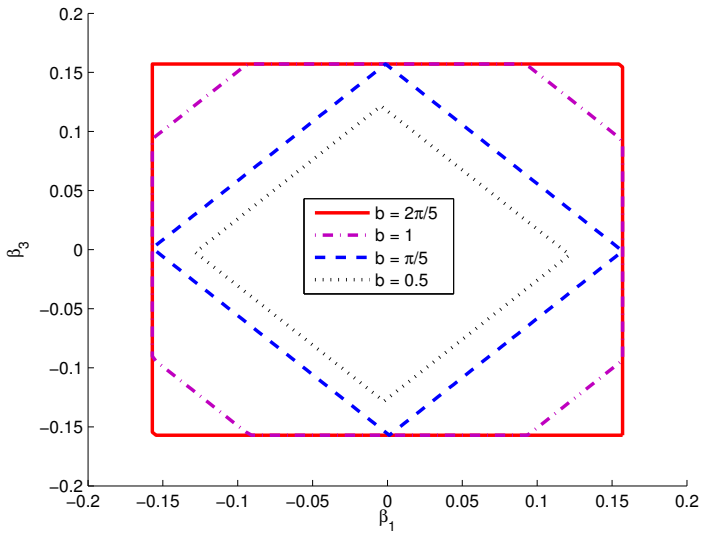

Figure 3: Phase portraits of the strokes for small amplitudes, $a = \pi/20$. The shapes observed are consistent with the discussion in section 3.

5.2 Comparison with the classical Purcell swimmer

Now we compare the performance of the optimal swimmer with respect to the classical Purcell swimmer defined by $L = 1, L_2 = 2$, meaning a ratio of 2. For this comparison we set $a = \pi/6$ (thus a stroke amplitude of $\pi/3$) and $b = \pi/3, 2\pi/3, \pi, 4\pi/3$ and $T = 1$. The optimization for the Purcell swimmer is done by setting $L = 1$ instead of letting it free. The results are summed up in Table.2 and Fig.4. We see that the shape of the stroke matches the empirical law, and that the optimal link ratio stays close to its theoretical value. We also observe a consistent gain in displacement that seems to increase with the speed limit, up to 64% for the classical Purcell stroke (square).

Table 2: Optimal swimmer vs Purcell swimmer.

b	x(T)	L_2/L	stroke	$x_{Purcell}(T)$	gain
$pi/3$	1.17E-2	0.717	diamond	7.373E-3	51%
$2\pi/3$	4.57E-2	0.708	diamond	2.848E-2	60%
π	7.82E-2	0.699	octagon	4.806E-2	63%
$4\pi/3$	8.80E-2	0.695	square	5.359E-2	64%

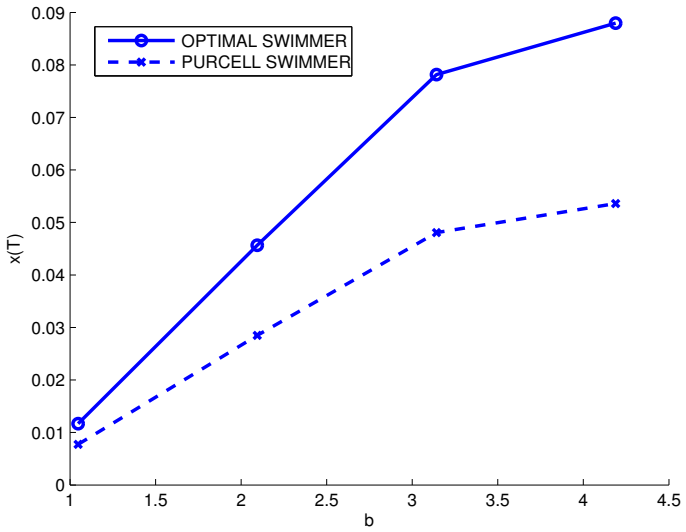

Figure 4: Displacement for the optimal/Purcell swimmer.

5.3 Large amplitudes, influence of angle limits

Now we study the influence of the maximal amplitude of the stroke, set by the bound a. In this last part we set the deformation speed limit $b = 1$ to focus on the amplitude. Since we would like to study only the true optimal strokes, whose period is not known, we also take a longer final time $T = 25$. We expect to obtain trajectories that exhibit a sequence of several identical strokes with a period $T^* < T$. The number of time steps is raised accordingly to 2500, which increases the computational time up to half an hour. Another way of finding the optimal stroke directly could be to leave the final time T free in the optimization, while maximizing the average speed of the stroke $x(T)/T$ instead of the displacement $x(T)$.

The results are illustrated in Table.3 and Figs.5-6. First, the simulations confirm that the optimal strategy is a periodic sequence of identical strokes. The shape of the optimal stroke is always octagonal until it becomes unconstrained for very large values of a. We observe that the central symmetry observed for small amplitudes is lost for larger a, however symmetry w.r.t both diagonal axes still holds as expected.

In the unconstrained case, we see arcs that are neither bang arcs (diagonal) or constrained arcs (horizontal/vertical), but rather appear as smooth curves (see Fig.5) . These are characteristic of so-called *singular arcs*, namely the case where $\langle p, g_i(z)\rangle = 0$ in the PMP. More details on the analysis of singular arcs can be found in [20], unfortunately here the complexity of the

g_i makes further study quite difficult.

The total displacement $x(T)$ increases with a, first almost linearly when $a < \pi/3$ (see Fig.6). From $a \approx 1.95$ and above, we obtain the same, unconstrained solution. The improvement in displacement appears to be marginal between $a = \pi/3$ and the unconstrained case. Note that since the displacement is expected to be a monotone increasing function of a, we see that for $a = 1.5$, the optimization converged to a local solution.

The optimal ratio L_2/L shows a steady decrease with a, starting quite close to the value 0.721 computed for small amplitudes, the seemingly reaching a limit value of $2/3$ in the unconstrained case (i.e. $L = 1.5, L_2 = 1$). We recall that the classical Purcell swimmer has a link ratio of 2 ($L = 1, L_2 = 2$).

Table 3: Larger amplitudes: optimal link ratio and stroke. Solutions become unconstrained about $a = 1.95$.

a	x(T)	L_2/L	stroke
$\pi/20$	0.192	0.719	octagon x26
$\pi/10$	0.384	0.712	octagon x13
$\pi/6$	0.593	0.697	octagon x7
0.75	0.811	0.676	octagon x5
$\pi/3$	1.088	0.660	octagon x4
1.25	1.266	0.660	octagon x4
1.5	1.263	0.660	octagon x3
1.75	1.329	0.667	octagon x3
$2\pi/3$	1.335	0.667	unconstrained x3
2.5	1.335	0.667	unconstrained x3

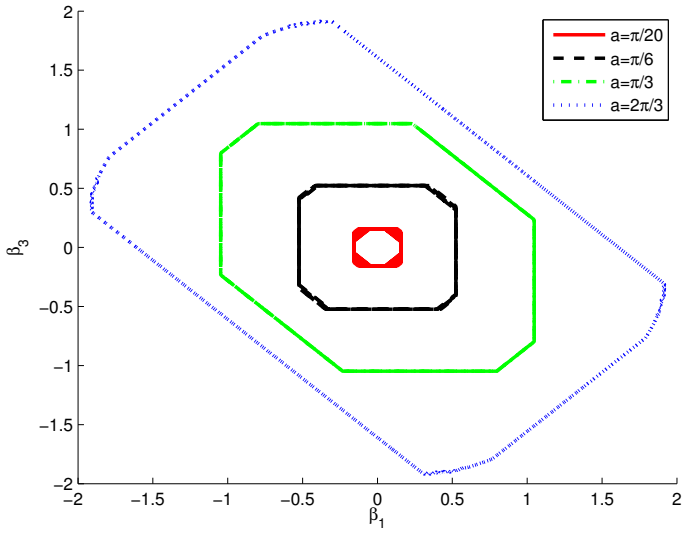

Figure 5: Larger amplitudes - Phase portrait (with several superposed strokes for each trajectory).

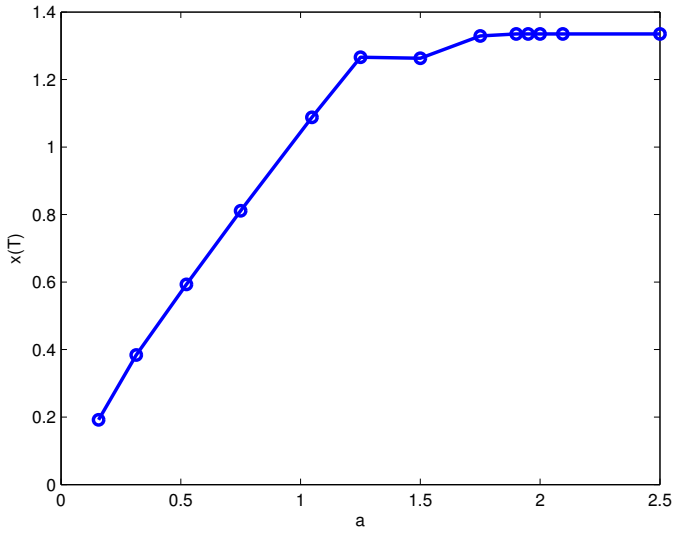

Figure 6: Larger amplitudes - Overall displacement. Note that since the displacement is expected to be a strictly increasing function of a, we see that for $a = 1.5$, the optimization converged to a local solution.

6 Conclusion

This study is devoted to the optimization of the link ratio of the three-link swimmer for maximal displacement. We provide an estimate of the displacement based on an expansion at small deformations, which gives a theoretical optimal link ratio. Numerical simulations when solving the optimal control numerically are consistent with this theoretical ratio for small amplitudes. We also observe that the optimal ratio changes for large amplitudes, with a limit value of 0.667 in the unconstrained case versus a theoretical ration of 0.721 at small amplitudes. For an amplitude of $\pi/3$, the displacement gain is about 60% compared with the classical Purcell swimmer design. A possible continuation of this work is the comparison of different objective functions, such as average speed or efficiency.

References

[1] A. A. Agrachev. *Non linear and optimal control theory.* Springer Verlag, 2008.

[2] F. Alouges, A. DeSimone, L. Giraldi, and M. Zoppello. Self-propulsion of slender micro-swimmers by curvature control: N-link swimmers. *Journal of Non-Linear Mechanics*, 56(132-141), 2013.

[3] J. E. Avron and O. Raz. A geometric theory of swimming: Purcell's swimmer and its symmetrized cousin. *New Journal of Physics*, 10(063016), 2008.

[4] L. E. Becker, S. A. Koehler, and H. A. Stone. On self-propulsion of micro-machines at low Reynolds number: Purcell's three-link swimmer. *J. Fluid Mech.*, 490:15–35, 2003.

[5] R. S. Berman, O. Kenneth, J. Sznitman, and A. M. Lishansky. Undulatory locomotion of finite filaments: lessons from caenorhabditis elegans. *New Journal of Physics*, 15, 2013.

[6] J.T. Betts. *Practical Methods for Optimal Control Using Nonlinear Programming*. Advances in design and control. Society for Industrial and Applied Mathematics, 2001.

[7] V.G. Boltyanskii, R.V. Gamkrelidze, and L.S. Pontryagin. Towards a theory of optimal processes. *Reports Acad. Sci. USSR*, 110(1), 1956.

[8] F. Bonnans, D. Giorgi, S. Maindrault, P. Martinon, and V. Grelard. Bocop - a collection of examples. Technical report, INRIA, http://www.bocop.org, 2014.

[9] C. Brennen and H. Winet. Fluid mechanics of propulsion by cilia and flagella. *Ann. Rev. Fluid Mech.*, 9:339–398, 1977.

[10] J. M. Coron. *Control and Nonlinearity*. American Mathematical Society, 2007.

[11] R. Dreyfus, J. Baudry, M. L. Roper, M. Fermigier, H. A. Stone, and J. Bibette. Microscopic artificial swimmers. *Nature*, 437:862–865, 2005.

[12] L. Giraldi, P. Martinon, and M. Zoppello. Controllability and optimal strokes for N-link micro-swimmer. *Proc. 52th Conf. on Dec. and Contr. (Florence, Italy)*, 2013.

[13] J. Gray and J. Hancock. The propulsion of sea-urchin spermatozoa. *Journal of Experimental Biology*, 32(802-814), 1955.

[14] E. Lauga and T. Powers. The hydrodynamics of swimming micro-organisms. *Rep. Prog. Phys.*, 72(09660), 2009.

[15] J. Lighthill. *Mathematical biofluiddynamic*. Society for Industrial and Applied, Philadelphia, Pennsylvania, U.S.A., 1975.

[16] R. Montgomery. *A tour of subriemannian geometries, theirs geodesics and applications*. American Mathematical Society, 2002.

[17] A. Najafi and R. Golestanian. Simple swimmer at low Reynolds number: Three linked spheres. *Physical Review E*, 69(6):062901, 2004.

[18] E. M. Purcell. Life at low Reynolds number. *American Journal of Physics*, 45:3–11, 1977.

[19] D. Tam and A. E. Hosoi. Optimal strokes patterns for Purcell's three link swimmer. *Physical Review Letters*, 98(068105), 2007.

[20] E. Trelat. *Contrôle optimal : théorie and applications*. Vuibert, Collection Mathématiques Concrètes, 2005.